Supporting information

Moving Behavior of Nanodroplets on Wedge-Shaped Functional Surfaces

Shuai Wang [a, c] Chao Wang [b, 1] Zhilong Peng [a, c] Shaohua Chen [a, c, 2]

[a] *Institute of Advanced Structure Technology, Beijing Institute of Technology, Beijing, 100081, China*

[b] *LNM, Institute of Mechanics, Chinese Academy of Sciences, Beijing, 100190, China*

[c] *Beijing Key Laboratory of Lightweight Multi-functional Composite Materials and Structures, Beijing Institute of Technology, Beijing, 100081, China*

[1]E-mail address: wangchao@lnm.imech.ac.cn (C.W).

[2]E-mail address: chenshaohua72@hotmail.com (S. C).

1. The mechanical mechanism of droplet moving on a wedge-shaped functional surface

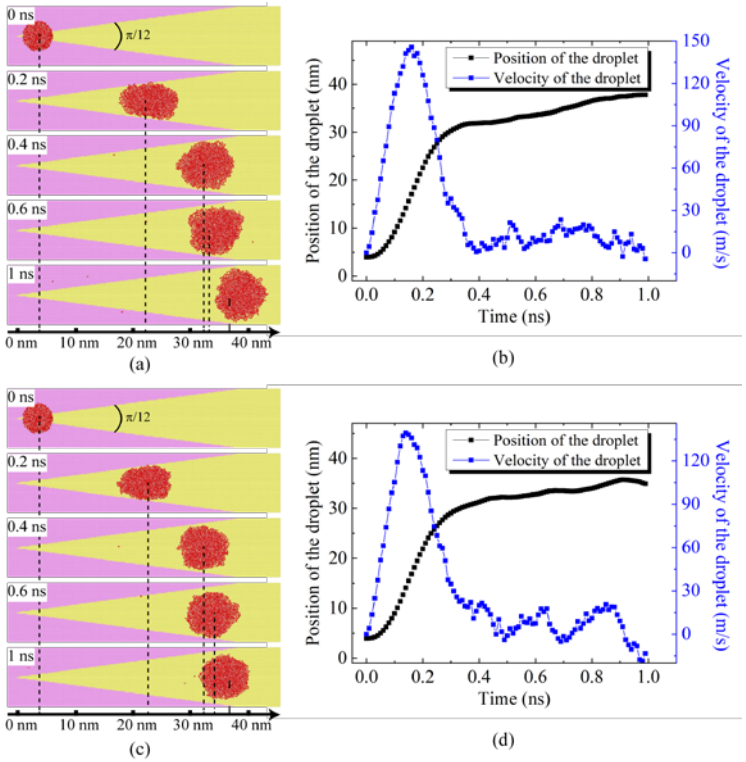

Figure S1. A water droplet moves spontaneously on a graphene sheet within an embedded wedge-shaped region. (a, c) Snapshots of the position of droplet on the wedge-shaped functional surface at 0, 0.2, 0.4, 0.6 and 1 ns; (b, d) Position and velocity of the water droplet as a function of the collapsed time. The diameter of the droplet *d* is 5 nm. The TIP3P model is adopted in (a) and (b), while TIP4P model is adopted in (c) and (d).

Different water models have different parameters in potential energy functions, thus may induce small differences in depicting water properties. Both the TIP3P model and TIP4P one are adopted as shown in Figure S1. Comparing both results and the present one based on SPC/E model, it is found that the motion tendency keeps the same with only small difference on values of the velocity. Such a result is because the

droplet motion is mainly actuated by the force between the droplet and substrate with wedge-shaped gradient regions.

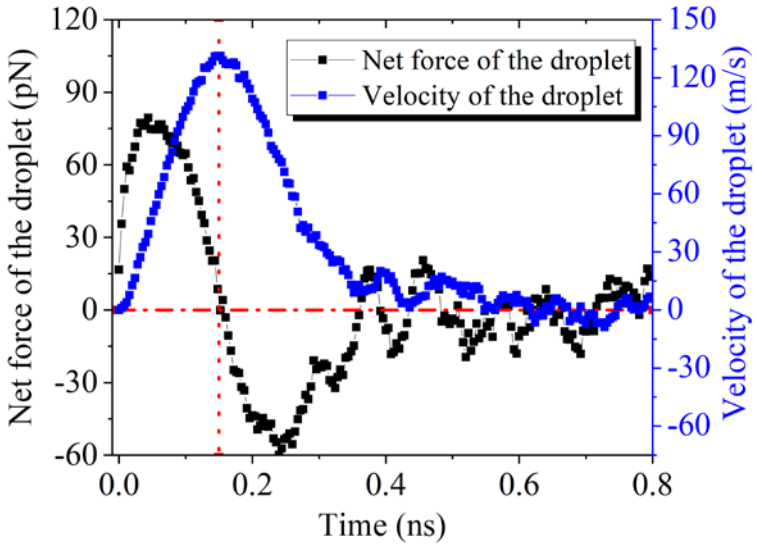

Figure S2. Net force and velocity of the water droplet as a function of the collapsed time. The diameter of the droplet *d* is 5 nm.

The droplet reaches its maximum velocity ~132.4 m/s at about 0.15 ns, the corresponding location on the functional surface and the configurations viewed from different directions at this moment are shown in Figure 2c.

The resultant net force of the droplet keeps positive at the initial moving stage and vanishes at about 0.15 ns as shown Figure S2. After that, the resultant net force becomes negative. As a result, the maximum velocity emerges at about 0.15 ns, after which the velocity would decrease. Such a result can be well explained with the understanding of mechanics.

The droplet is first relaxed separately at a constant temperature for a long time until both the volume and potential energy of the droplet keep nearly unchanged as

shown in Figure S3. It also shows that droplet has less fluctuation compared to a smaller one.

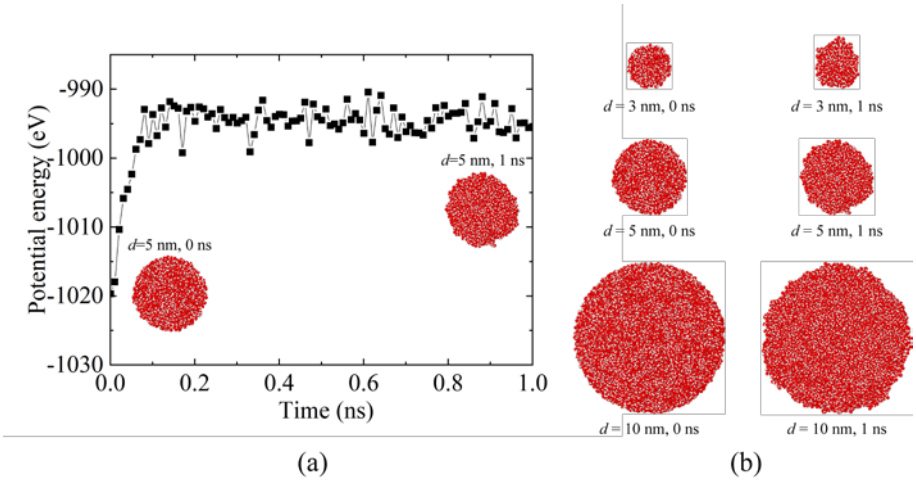

Figure S3. Energy minimization of droplet. (a) Variation of the potential energy of droplet during relaxation, the droplet diameter is 3 nm; (b) the initial and final configuration of droplet with diameter 3, 5 and 10 nm.

2 New techniques for tuning droplet motion

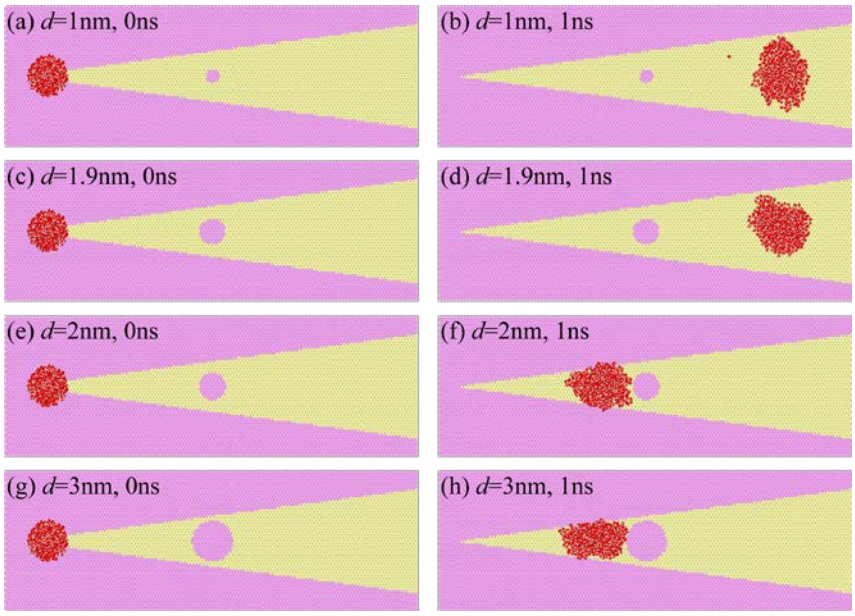

Figure S4. The pinning behavior of water droplet on different patterned surfaces. (a,c,e,g) The initial and (b,d,f,h) the final configuration of droplet on functional surface with different defect diameter. The droplet diameter is 3 nm.

For a droplet with diameter 3 nm, it is found that if the defect diameter is smaller

or equal to 1.9 nm, the droplet can move over the defect, however, if the defect diameter is larger than 1.9 nm (2 nm and 3 nm as typical examples), the droplet will be pinned near the defect.

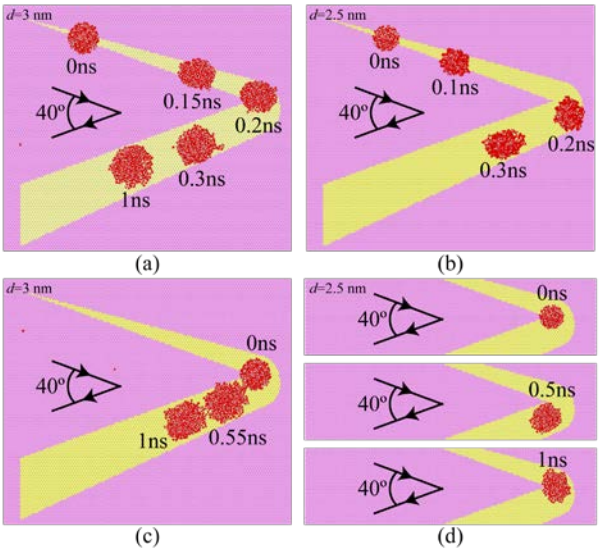

Figure S5 Nonlinear motion of a water droplet on a patterned surface. The corner angle of the curve page is 40°. The droplet with diameter (a) 3 nm or (b) 2.5 nm is placed the narrow end, the droplet with diameter (c) 3 nm or (d) 2.5 nm is placed near the corner.

The functional surface with 40 degrees wedge-shaped angle has been carefully designed, the droplet with diameter 3 nm even placed near the corner can even move over the corner, as shown in Figure S5a and c. The inertia of droplet does not need to play a role in this case. However, as shown in Figure S5b and d, for a droplet with diameter 2.5 nm, the droplet placed far from the corner can move over the corner while the droplet near the corner cannot.

3. Theoretical analysis of the driving force of a droplet moving on a single wedge-shaped functional surface

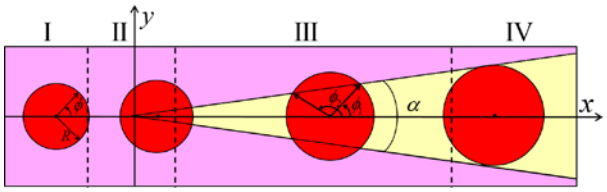

Figure S6. Theoretical model for calculating the driving force of a droplet moving on a single wedge-shaped functional surface

The theoretical model for calculating the driving force of droplets moving on a wedge-shaped functional surface is shown in Figure S6, where the yellow and pink regions represent the hydrophilic and hydrophobic surfaces, respectively. The red circle denotes the contact line of droplets on the surface. The origin of a rectangular coordinate system is placed at the wedge angle with the horizontal *x*-axis. *R* and ϕ are the radius and polar angle of the contact line, while α is the wedge angle of the hydrophilic region.

For simplicity, the contact line of droplet on the surface is assumed to be spherical cap with constant volume. When the droplet is contained completely in hydrophilic or hydrophobic region, the corresponding contact radius R_1 or R_2 can be easily calculated according to the contact angle and volume.

$$R_1 = \sqrt[3]{\frac{4}{(2+\cos\theta_1)(1-\cos\theta_1)^2}}\frac{d}{2}\sin\theta_1 \tag{S1}$$

$$R_2 = \sqrt[3]{\frac{4}{(2+\cos\theta_2)(1-\cos\theta_2)^2}}\frac{d}{2}\sin\theta_2 \tag{S2}$$

where θ_1 and θ_2 denote the equilibrium contact angles in the hydrophilic and hydrophobic region, respectively. The parameter *d* is diameter of the spherical droplet in MD simulation.

We assume the droplet radius linearly increase from R_2 to R_1 as the droplet move from hydrophobic region to the hydrophilic one, the droplet radius can be written as:

$$R = \frac{R_1 - R_2}{R_2 \sin(\alpha/2) + R_1} \sin(\alpha/2) x_0 + \frac{R_1 R_2 \sin(\alpha/2) + R_1 R_2}{R_2 \sin(\alpha/2) + R_1} \tag{S3}$$

If the trailing side is on the hydrophilic vertex, the contact radius R_0 can be written as:

$$R_0 = \frac{R_1 R_2 \left(1 + \sin(\alpha/2)\right)}{R_1 \left(1 - \sin(\alpha/2)\right) + 2R_2 \sin(\alpha/2)} \tag{S4}$$

According to the position of droplet, the surface can be divided into four regions to find the corresponding driving force acted on droplet, as shown in Figure S6. For all four regions, the driving force can be uniformly written as,

$$F_{\mathrm{d}} = 2\int_0^{\pi R/2} \left[\left(\gamma_{\mathrm{SG}} - \gamma_{\mathrm{SL}}\right)_{\mathrm{f}} - \left(\gamma_{\mathrm{SG}} - \gamma_{\mathrm{SL}}\right)_{\mathrm{r}} \right] \cos\phi dl \tag{S5}$$

where γ_{SG} and γ_{SL} denote the solid-gas and solid-liquid interfacial tension, respectively. The subscripts f and r correspond to "front" and "rear", respectively. In this model, "front" denotes the right contact line and "rear" is the left one.

Young's equation is as follows,

$$\gamma_{\mathrm{SG}} - \gamma_{\mathrm{SL}} = \gamma \cos\theta \tag{S6}$$

where θ denotes the local equilibrium contact angle and γ is the liquid-gas interfacial tension. Then, the driving force can be rewritten as,

$$F_{\mathrm{d}} = 2R\gamma \int_0^{\pi/2} \left[\cos\theta_f - \cos\theta_r \right] \cos\phi d\phi \tag{S7}$$

In regions I and IV, ϕ_{r} and ϕ_{f} in Eq. (S3) equal θ_2 and θ_1, respectively, resulting a vanishing driving force.

In region II, the contact line has two intersection points with the boundary between the hydrophobic and hydrophilic areas. Let

$$y = \tan\frac{\alpha x}{2} \tag{S8}$$

$$x = R\cos\phi + x_0,\ y = R\sin\phi \tag{S9}$$

We obtain the polar angle of the intersection point:

$$\phi_1 = \arcsin\left(\frac{\sin(\alpha/2)}{R}x_0\right) + \alpha/2\,. \tag{S10}$$

where x_0 denotes the position of droplet center.

Note the symmetric feature of the model. The driving force can be written as,

$$F_{\mathrm{d}} = 2R\gamma\left(\cos\theta_1 - \cos\theta_2\right)\sin\phi_1 \tag{S11}$$

Similarly, in region III, the driving force can be yielded as

$$F_{\mathrm{d}} = 2R\gamma\left(\cos\theta_1 - \cos\theta_2\right)\left(\sin\phi_1 - \sin\phi_2\right) \tag{S12}$$

where ϕ_2 is the second solution obtained from Eq. (S8-9) and can be expressed as,

$$\phi_2 = \pi - \arcsin\left(\frac{\sin(\alpha/2)}{R}x_0\right) + \alpha/2 \tag{S13}$$

Finally, the driving force as a function of *x*-coordinate can be written as

$$F_{\mathrm{d}} = \begin{cases} 0,\ \left(\mathrm{I}: x_o < -R_2\right) \\ 2R\gamma\left(\cos\theta_1 - \cos\theta_2\right)\sin\phi_1,\ \left(\mathrm{II}: -R_2 \le x_0 < R_0\right) \\ 2R\gamma\left(\cos\theta_1 - \cos\theta_2\right)\left(\sin\phi_1 - \sin\phi_2\right),\ \left(\mathrm{III}: R_0 \le x_0 < R_1/\sin(\alpha/2)\right) \\ 0,\ \left(\mathrm{IV}: x_0 \ge R_1/\sin(\alpha/2)\right) \end{cases} \tag{S14}$$

4. The effect of droplet size and wedge angles on the moving behavior

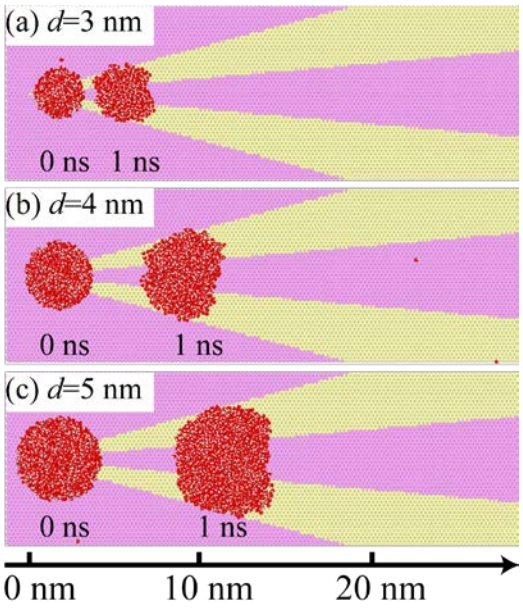

Figure S7. The pinning behavior influenced by the diameter of droplets. The droplet diameters are (a) 3nm, (b) 4nm and (c) 5nm, respectively. The wedge angle of both the hydrophilic and hydrophobic zones equals $\pi/12$.

Further simulations indicate that the diameter of droplets could greatly influence the pinning position as shown in Figure S7. It shows that the larger the size of droplets, the farther the droplet will be pinned. In addition, both the wedge angle of the hydrophilic zone and that of the hydrophobic zone will show significant influence on the pinning position as shown in Figure S8. It exhibits that the smaller the wedge angle of the hydrophilic area or the hydrophobic one, the farther the droplet will be pinned.

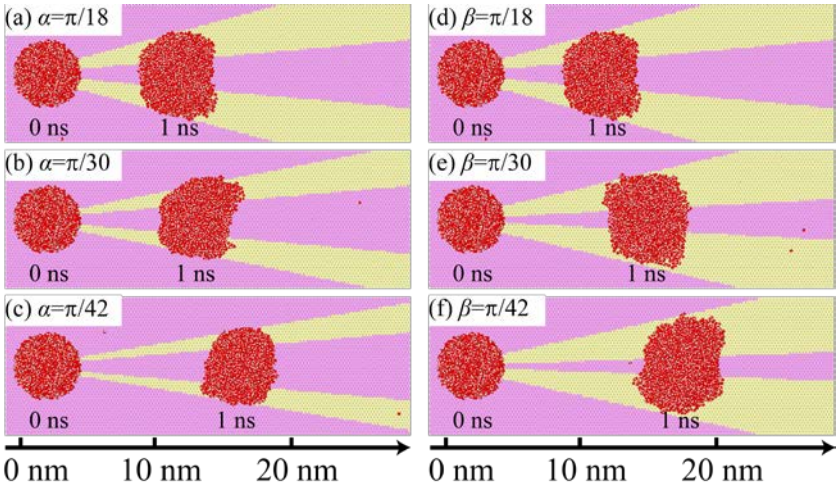

Figure S8. The effect of wedge angles on the pinning position. (a-c) Different wedge angles of the hydrophilic zone α on the pinning position, while the wedge angle of the hydrophobic zone $\beta=\pi/18$ keeps unchanged. (d-f) Different wedge angles of the hydrophobic zone β on the pinning position, while $\alpha=\pi/18$ is fixed.